Chapter 5

Diffusion and bistability

Abstract In the previous chapter, diffusion under reaction conditions was studied at steady state and above 440 K, where the experiments do not show kinetic bistability. Strong variations of the local reactant fluxes at the surface were found, which induce strong variation of the local x_{CO} over the surface. For $x_{CO} = 0.45$, for example, the local values are typically between 0.3 on the side of the particle facing the O_2 beam and 0.8 on the shaded side. That is, the initial local reaction conditions at the particle surface vary between O-rich and CO-rich (without diffusion). Therefore, the local reactant coverages established at transient or steady state are expected to be critically dependent on F_{CO}, which governs Θ_{CO}, and L_O and τ_O, which govern the local Θ_O.

The bistability of the reaction depends on the reaction conditions (i.e. T and x_{CO}). The morphology of the particles as well as diffusion are therefore expected to play a role in the bistable behavior. In this chapter, we propose to study the interplay between diffusion processes and bistability.

5.1 Global reaction rates at steady state

Figure 5.1a displays CO_2 production rates at steady state simulated by RD. The results of RD quantitatively reproduce the experimental data both as a function of x_{CO} and T (from 400 to 490 K) as well as the width and temperature region of the bistability. All deviations in x_{CO} are within the limits of experimental error.

Another model, based on RD is elaborated, which cancels diffusion. F_{CO} and F_{O_2} onto the particle surface are averaged to $\overline{F_{CO}}$ and $\overline{F_{O_2}}$. These averaged fluxes are then used in RD. Since there are no differences in the local fluxes anymore, the gradient in Θ_O disappears as well. Diffusion is suppressed but the morphology of the particle is kept. In the following, we call this homogeneous flux model (HF).

Figure 5.1 shows comparisons between both models. Despite the strong Θ_O gradient under CO-rich conditions for RD, the differences in global rate are very small under all conditions of T and x_{CO} (Figure 5.1a and b). The shift of the bistability region is also minor (Figure 5.1c). Indeed, the differences between the two models are typically within experimental accuracy. These results show that for the present type of model catalyst, effects arising from the inhomogeneous distribution of reactants do not lead to significant

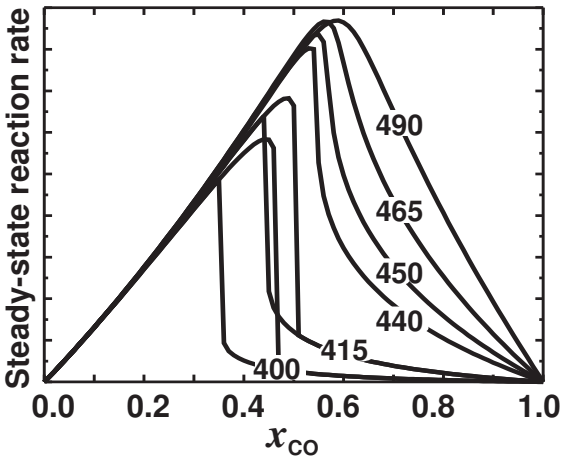

(a) RD, $E_{diff} = 55\,kJ\,mol^{-1}$

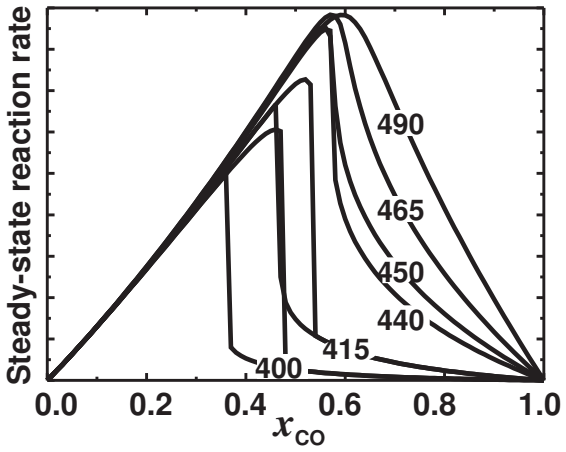

(b) HF

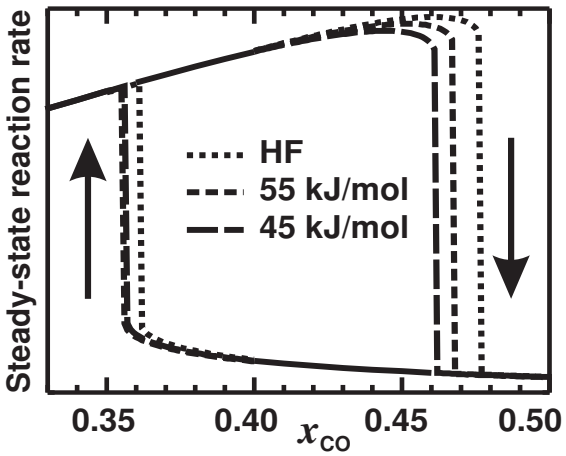

(c) $T = 400\,K$

Figure 5.1. Global CO oxidation rates simulated obtained from two different models: (a) RD and (b) HF. (c) The bistable regime is investigated for $T = 400\,K$ with RD, $E_{diff} = 45$ and $55\,kJ\,mol^{-1}$, and HF.

changes of activity. Therefore, effects related to the local variations of the reaction rates cannot be identified via AI measurements.

O-rich conditions The residence times of O_{ad} and CO_{ad} at the timescale of the reaction are long. Both species can therefore diffuse to the shaded side of the particles. As a result, we expect equilibration of the coverages and RD and HF should yield very similar results.

CO-rich conditions First considering O_{ad}, Θ_O is small and shows a pronounced gradient over the particle. The low O_{ad} coverage implies a reduced residence time at the timescale of the experiments. Then, results expected from RD and HF should differ, which is not the case. Under CO-rich conditions, the RDS is the dissociative adsorption of O_2. The inhibitor effect of CO_{ad}, however, implies that the O_2 adsorption probability is primarily determined by Θ_{CO}. But CO_{ad} diffuses fast at the timescale of the reaction and Θ_{CO} is equilibrated over the particle regardless of the Θ_O gradient (there is no O_{ad} poisoning). The RDS of the reaction thus depends on

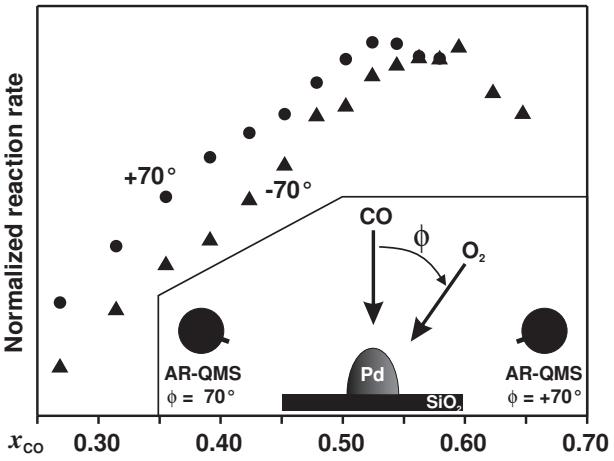

Figure 5.2. Local CO oxidation rates (experiments) measured at $\phi = 70°$ and -70°, $T = 465$ K by the AR QMS; inset: experimental setup.

Θ_{CO} and not on Θ_O. Since Θ_{CO} is averaged by diffusion in RD and by design in HF, both models yield similar results.

Bistability window We observe a well-defined transition between the two regimes upon leaving the bistability window. This indicates that fast diffusion of CO_{ad} over the particle likely leads to synchronization of the switching behavior over the whole particle.

5.2 Local reaction rates at steady state

5.2.1 Experiments

AI mass spectrometry does not provide information on local variations of the reaction rate. We therefore propose measurements of the local reaction rates by AR mass spectrometry. For this experiment, detection angles of $\phi = -70°$ and $\phi = 70°$ are chosen where the reaction rate is measured versus x_{CO}. That is, on the side facing the O_2 beam and on the shaded side. The reaction rates are displayed in Figure 5.2, normalized to their maximum value. For both detection angles, the maximum rate indicates the transition between O-rich and CO-rich. The position of this maximum is slightly shifted between the two detection angles. It occurs at $x_{CO} = 0.53 \pm 0.02$ for $\phi = -70°$ and $x_{CO} = 0.58 \pm 0.02$ for $\phi = 70°$.

The change in the transition point is small compared to the drastic variations of x_{CO} at the surface of the particle (cf. Section 4.2.1). This indicates that the transition between the reaction regimes occurs in a largely synchronized fashion over the entire particle surface. As mentioned above, the synchronization is attributed to fast diffusion of CO_{ad} over the surface.

5.2.2 Simulations

In order to farther explore the switching behavior between the reaction regimes, we perform simulations of the local reaction rates as a function of x_{CO}, both below the critical

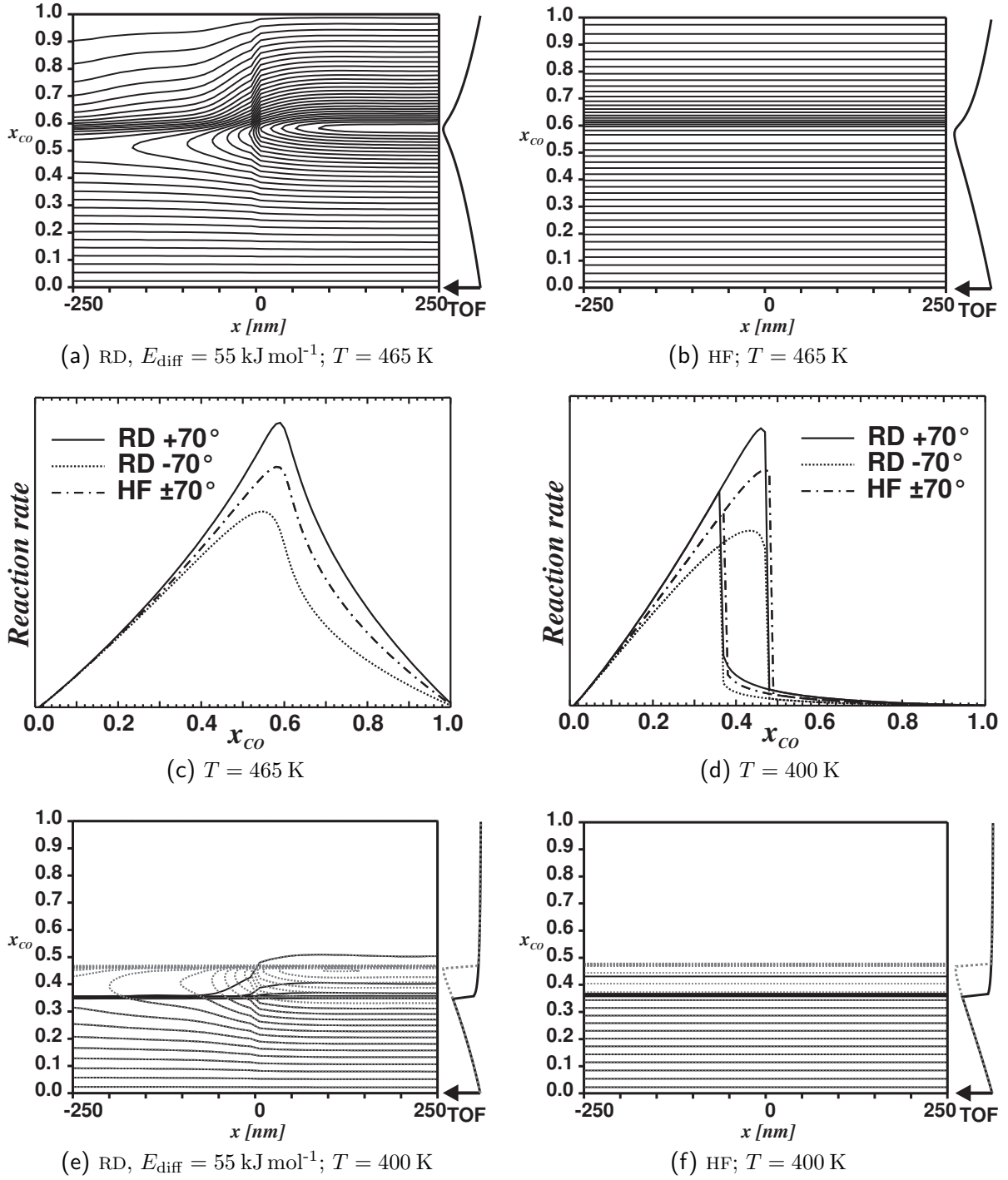

(a) RD, $E_{\text{diff}} = 55\,\text{kJ}\,\text{mol}^{-1}$; $T = 465\,\text{K}$

(b) HF; $T = 465\,\text{K}$

(c) $T = 465\,\text{K}$

(d) $T = 400\,\text{K}$

(e) RD, $E_{\text{diff}} = 55\,\text{kJ}\,\text{mol}^{-1}$; $T = 400\,\text{K}$

(f) HF; $T = 400\,\text{K}$

Figure 5.3. Simulations (RD and HF) of the local reaction rate along the O_2 beam direction are plotted on contour plots for $0 < x_{\text{CO}} < 1$ [(a)–(b) and (e)–(f)]. The global (integrated) reaction rate is also presented [(c)–(d)].

temperature, i.e. in the presence of a bistability window, and above the critical temperature, i.e. in absence of kinetic bistability.

- $T = 465\,\mathrm{K}$, above the bistable regime. The reaction rates obtained from HF are plotted in Figure 5.3b. They are independent of the position on the particle and increase linearly with increasing x_{CO} until $x_{\mathrm{CO}} = 0.6$. Then, the transition to the CO-rich regime is reached and the reaction rates drop rapidly. The reaction rates obtained from RD are plotted on Figure 5.3a. There are nearly no gradients in the local reaction rates in the limit of small x_{CO}. For $x_{\mathrm{CO}} > 0.3$, however, the gradients become successively larger. In the vicinity of the transition point, the rates on the shaded side of the particle are only slightly dependent on x_{CO}. Whereas they increase strongly on the side facing the O_2 beam. This effect is related to a pronounced decrease in Θ_{O}. And it leads to a strong decrease in L_{O}. As a result, the maximum reaction rates appear at slightly different x_{CO} values on both sides of the particle. This observation is in full agreement with the experimental results.

- $T = 400\,\mathrm{K}$, in the bistable regime (see Figure 5.3d–f). The behavior upon switching between the regimes is very similar to the situation at higher temperatures. Close to the transition point, the gradient in the reaction rate increases rapidly as a result of decreasing τ_{O}. This gives rise to a maximum in the rate appearing at slightly different x_{CO}. The actual transition to CO-rich, however, occurs at a well-defined x_{CO} in a synchronous fashion over the complete particle surface. The same applies for the transition from CO-rich to O-rich.

In order to compare directly with the experiments, the effective reactant flux for the two detection angles is calculated Figure 5.3c and d. It is found that the shift of the maximum rate as a function of the detection angle is very well reproduced by RD. This again supports the previous suggestion that the transition between the two reactive states is mainly triggered and synchronized by Θ_{CO} and fast $\mathrm{CO}_{\mathrm{ad}}$ diffusion over the particle.

5.3 Global reaction rates under transient conditions

5.3.1 Experiments

Figure 5.4 displays representative experimental results for the transient-kinetics reaction rates. The data are obtained using a modulated O_2 beam and a continuous CO beam (i.e. steady state, with both beams operating, is approached starting from a CO-precovered surface) and using a modulated CO beam and a continuous O_2 beam (i.e. steady state is approached from an O-precovered surface).

CO-precovered Figure 5.4a shows two characteristic types of transients. In the O-rich regime, the reaction rate has a steep maximum after admission of the O_2 beam before reaching the steady state. And the CO_2 production at steady state increases linearly with x_{CO}. As x_{CO} approaches the transition to CO-rich, the time after which the transient maximum is observed increases. Simultaneously, the height of the

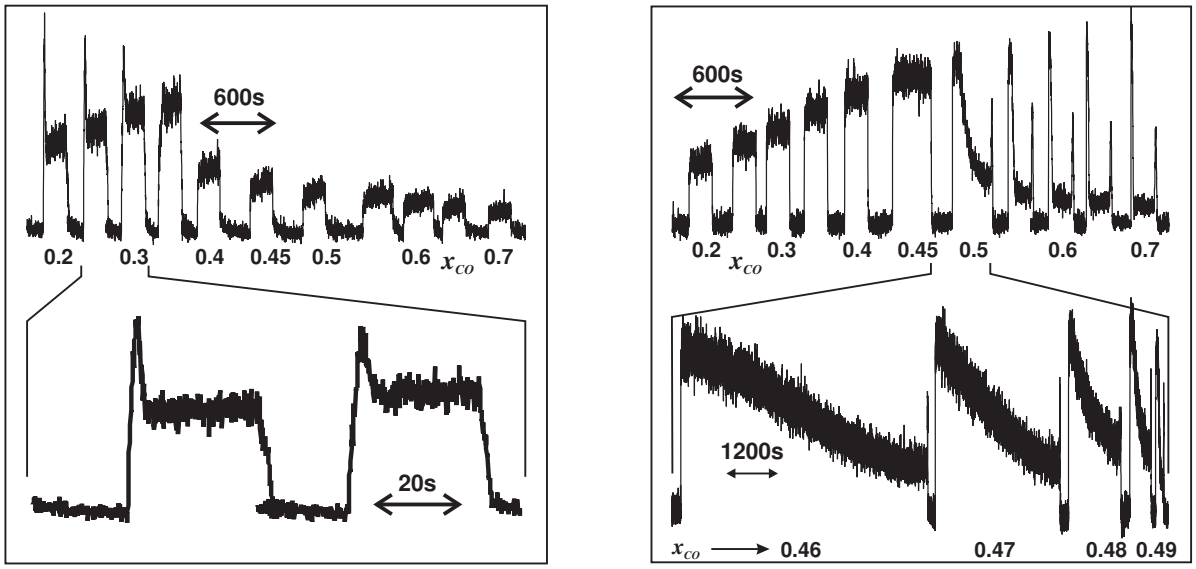

(a) CO-precovered surface (b) O-precovered surface

Figure 5.4. CO_2 transient measured at $T = 400\,K$ on (a) a CO-precovered surface (b) a O-precovered surface.

maximum decreases linearly with x_{CO}. Upon switching to CO-rich, a steep decrease in the rate occurs and the transient maximum in CO_2 production disappears. In the CO-rich regime, the steady state is reached monotonously. Then, the CO_2 production at steady state decreases, as well as the timescale on which it is reached.

O-precovered Figure 5.4b shows different transient behaviors. Both under O-rich and CO-rich conditions, the reaction rate instantaneously increases upon admission of CO (typically in the order of 50 ms). Under O-rich conditions, this maximum is also the steady state. Under CO-rich conditions, however, the maximum is followed by a slower transient and finally, a smaller steady state is reached. A second maximum appears after termination of the beam (discussed in [86, 92, 101]). In the vicinity of the bistability region, the timescale at which the steady states are reached diverges (Figure 5.4b). For example, at $0.49 \geqslant x_{CO} \geqslant 0.46$, transient times in the order of 10^3 to 10^4 s are measured.

5.3.2 Simulations

The transients are simulated by the microkinetic models RD and HF. Figure 5.5 compares RD and HF for a CO-precovered surface (Figure 5.5a and b) and an O-precovered surface (Figure 5.5c) below the critical temperature for five reaction regimes:

O-rich regime ($x_{CO} \leqslant 0.3$) The CO-precovered case exhibits a single transient maximum. From the coverages plotted in Figure 5.5, we see that the maximum CO_2 production occurs when Θ_{CO} decreases and Θ_O increases rapidly. The product of both quantities determines the reaction rate in the models and passes through a

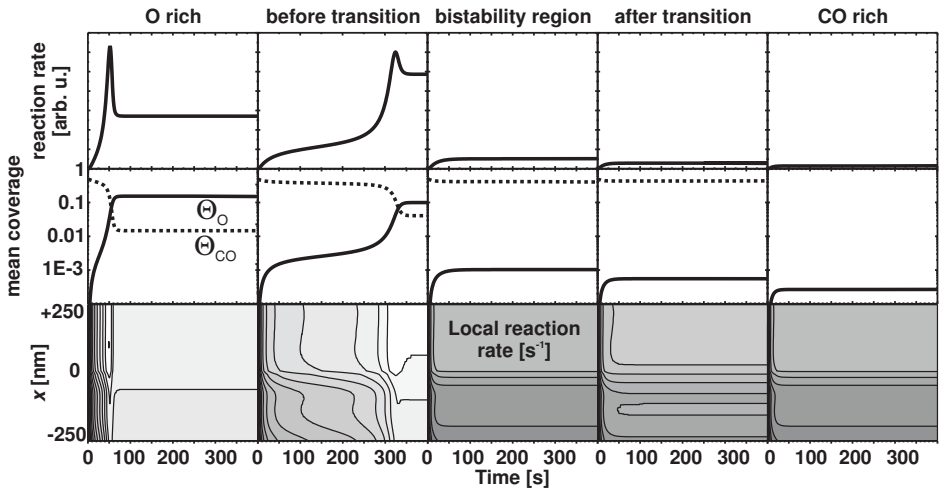

(a) RD, $E_{\mathrm{diff}} = 55\,\mathrm{kJ\,mol^{-1}}$; $T = 400\,\mathrm{K}$; CO-precovered surface

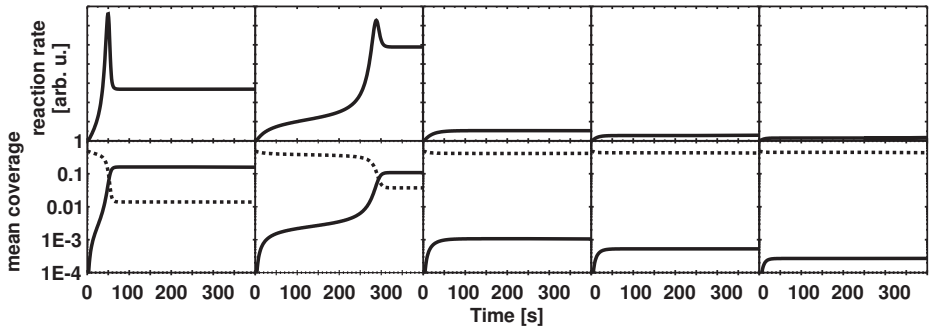

(b) HF; $T = 400\,\mathrm{K}$; CO-precovered surface

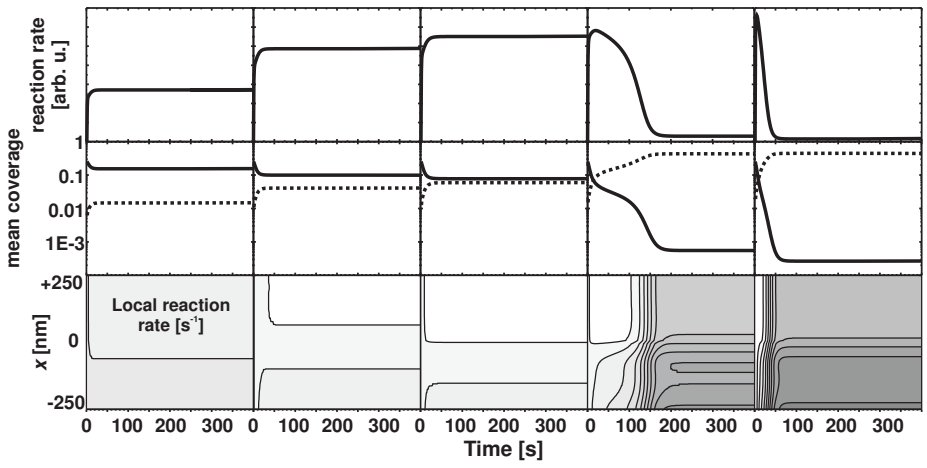

(c) RD, $E_{\mathrm{diff}} = 55\,\mathrm{kJ\,mol^{-1}}$; $T = 400\,\mathrm{K}$; O-precovered surface

Figure 5.5. Time evolution of the CO_2 production (first row); mean coverages (second row) and local reaction rates (third row, RD) for $x_{\mathrm{CO}} = 0.2$ (first column), 2% before the bifurcation (second column, $x_{\mathrm{CO}} = 0.35$, RD; $x_{\mathrm{CO}} = 0.353$, HF); in the bistable region, $x_{\mathrm{CO}} = 0.4$ (third column); 2% after the bifurcation (4th column, $x_{\mathrm{CO}} = 0.477$, RD; $x_{\mathrm{CO}} = 0.487$, HF) and $x_{\mathrm{CO}} = 0.6$ (5th column). The local reaction rates for RD are shown as a grayscale, decoding the reaction rate on a logarithmic scale. Again, the rate is shown for a cross-section of the particle containing the xz-plane.

maximum. Thereafter, the decrease in Θ_{CO} dominates over the increase in Θ_O, leading to a decrease in the global reaction rate. For the O-precovered case, the coverages rapidly and monotonously reach their steady-state values. Θ_O remains high, whereas Θ_{CO} remains low. Hence a fast and monotonous transient.

O-rich regime, near the transition The models reproduce well the divergence observed experimentally for the CO-precovered case. And the time required to establish the steady state increases as the transition approaches. The evolution of the coverages (Figure 5.5) shows that the first state reached from a CO-precovered surface is actually CO-rich (high Θ_{CO}, low Θ_O). The system then remains in that state for a certain time, which can exceed 100 s (steady state is reached in about 10 s in the CO-rich regime). But this state is unstable and the system slowly drifts toward lower Θ_{CO} and higher Θ_O until a rapid transition to O-rich occurs. For the O-precovered case, the first state reached is O-rich (high Θ_O, low Θ_{CO}). This state is stable and therefore constitutes the steady state.

Within the bistability region ($x_{CO} = 0.4$) As expected, both models predict two stable states: CO-rich is reached from a CO-precovered surface and O-rich from an O-precovered surface. Both states are kinetically stable, i.e., there is no change in the coverages after establishment of the regime. Both states are therefore steady.

CO-rich regime, near the transition The situation is the reverse of the second point. From a CO-precovered surface, the first regime encountered is CO-rich (high Θ_{CO}, low Θ_O), which is stable. However, the first regime encountered from an O-precovered surface is O-rich (high Θ_O, low Θ_{CO}). The O-rich regime, however, remains a relatively long time during which the coverages drift to lower Θ_{CO} and higher Θ_O. For certain coverage values, a rapid transition to the stable CO-rich regime occurs and the steady state is reached.

CO-rich regime ($x_{CO} \geqslant 0.5$) The situation is the reverse from the O-rich regime. For the CO-precovered case, a steady CO-rich regime is reached fast and monotonously. For the O-precovered case, a maximum in production rate appears when Θ_{CO} increases and Θ_O decreases rapidly. Then, farther decrease in Θ_O reduces the reaction rate until the steady state is reached. Similarly to the O-rich regime, the transient response becomes faster with increasing distance from the bistability region.

Remarks

- The situation under CO-rich conditions is not exactly the reverse of O-rich (esp. compare O-rich–CO-precoverage and CO-rich–O-precoverage). The transient maximum is reached immediately for the O-precovered situation. Whereas for the CO-precovered situation, it occurs after a delay (typically in the order of 10 s) upon admission of the complementary beam. Taking into account the discussion in Section 3.3, this results from the differences between the sticking coefficients of CO and O_2. Indeed, the sticking coefficient of CO is rather independent of Θ_O and it is high, even on an O-precovered surface (no O_{ad} poisoning). However, the sticking

coefficient of O_2 depends strongly on Θ_{CO}. Therefore, when CO adsorption is the RDS, i.e., under O-rich conditions, the precoverage of the surface does not inhibit the reaction rate. On the contrary, CO adsorbs fast on an O-precovered surface and the reaction probability is then very high. Hence CO_2 production is the highest immediately after admission of the CO beam, when Θ_O is the highest. Conversely, when O_2 adsorption is the RDS, i.e., under CO-rich conditions, CO-precoverage inhibits O_2 adsorption. And therefore the production rate is low in the beginning. Then, reaction slowly removes CO from the surface, which facilitates O_2 adsorption. As the RDS is accelerated, the reaction rate increases. And the transient maximum occurs for optimal values of Θ_{CO} and Θ_O.

- Here again, RD and HF do not yield significant differences. The reason for this behavior of the transient is the same as at steady state (cf. Section 5.1 and 5.2). Briefly, for the O-precovered case, CO_{ad} and O_{ad} diffuse rapidly at the timescale of their surface residence time. This leads to an equilibration of the coverages and the gradient in Θ_O vanishes. However, for the CO-precovered situation, the initial Θ_O gradient is large, indicating a drastically reduced τ_O and L_O. The gradient decreases as Θ_O increases. But still, the behavior of the global transient and of the average coverages develops similarly for both models. This indicates that fast diffusion of CO_{ad} results in a coupling of the transient response over the complete particle surface. Synchronization of the switching over the particle surface is also attributed to a coupling of the surface elements by the fast diffusion of CO_{ad} for RD. This results in a similar global transient response for both RD and HF.

Concerning the comparison to the experiments Section 5.3.1, all characteristic features of the transient experiments are well reproduced by the simulations. This holds not only for the general type of transient behavior but also for the details discussed above. In general, it can be concluded that for the present type of model catalyst the global transient kinetics are well described by both models. Whereas an accurate description of the local reaction rates on the particle surface requires an explicit description of diffusion processes by RD simulations.

5.4 Summary

We have investigated the local and global kinetics of CO oxidation on Sample C [$Pd/SiO_2/Si(100)$ prepared by EBL, 500 nm diameter, 450 nm height]. Employing molecular beam methods and angle-integrated and angle-resolved mass spectrometry, the local and global reaction kinetics were probed under steady state and transient conditions. Both, monostable and bistable regimes were investigated. The experimental results were analyzed in terms of two types of microkinetic models. A microkinetic mean field model assuming an homogeneous surface and an homogeneous reactant flux distribution (HF) and a detailed reaction–diffusion model (RD). Both models take into account the morphology of the catalyst, the geometry of the molecular-beam experiment as well as scattering form the support.

Global steady-state kinetics In spite of strong local variations of the reactant fluxes over the particle surface and limited oxygen mobility, it is found that the global reaction rates show temperature and flux dependences similar to single crystal studies. Also in analogy to single crystals, a well-defined bistability window is observed. The results are quantitatively reproduced by both RD and HF. The existence of the bistability is attributed to coupling of the surface coverages and reaction rates over the particle surface via fast CO_{ad} diffusion. As a result, the switching between the regimes occurs over the full surface of the particle at a well-defined ratio of reactant fluxes.

Local steady-state kinetics Local reaction rate measurements via AR mass spectrometry show a nearly synchronous switching behavior between O-rich and CO-rich over the full particle surface. On the basis of microkinetic simulations it is shown that the transition between the kinetic regimes is largely driven by surface mobility of CO_{ad}. In spite of the synchronous kinetic phase transition, pronounced gradients of oxygen coverage and reaction rate persist over the particle surface under CO-rich conditions. This effect, which is the result of the limited oxygen diffusion length, can only be quantitatively described by RD.

Global transient kinetics Different types of transient behaviors are observed in various kinetic regimes, i.e. under CO-rich, in the bistable regime and under O-rich conditions, depending on the initial coverage of the surface (either O- or CO-precovered). All characteristic types of global transient behavior are well described by HF, whereas a description of the local rate distribution over the particle surface requires a reaction–diffusion model.